OXFORD CDE

Journal of Computational Design and Engineering, 2022, **9**, 2297–2313

DOI: 10.1093/jcde/qwac107
Advance access publication date: 8 October 2022
Research Article

Twisted-fin parametric study to enhance the solidification performance of phase-change material in a shell-and-tube latent heat thermal energy storage system

Liu Bo[1], Jasim M. Mahdi[2], Alireza Rahbari[3], Hasan Sh. Majdi[4], Yi Xin[1], Wahiba Yaïci[5] and Pouyan Talebizadehsardari[6,*]

[1]College of Safety Science and Engineering, Xi'an University of Science and Technology, Xi'an 710054, China
[2]Department of Energy Engineering, University of Baghdad, Baghdad 10071, Iraq
[3]School of Engineering, the Australian National University, Canberra ACT 2601, Australia
[4]Department of Chemical Engineering and Petroleum Industries, Al-Mustaqbal University College, Babylon 51001, Iraq
[5]CanmetENERGY Research Centre, Natural Resources Canada, 1 Haanel Drive, Ottawa (Ontario), Canada
[6]Centre for Sustainable Energy Use in Food Chains, Institute of Energy Futures, Brunel University London, Kingston Lane, Uxbridge, Middlesex, UB8 3PH, UK
*Corresponding author. E-mail: pouyan.talebizadehsardari@brunel.ac.uk

Abstract

Phase change material (PCM) is considered as one of the most effective thermal energy storage (TES) systems to balance energy supply and demand. A key challenge in designing efficient PCM-based TES systems lies in the enhancement of heat transmission during phase transition. This study numerically examines the privilege of employing twisted-fin arrays inside a shell-and-tube latent heat storage unit to improve the solidification performance. The presence of twisted fins contributes to the dominating role of heat conduction by their curved shapes, which restricts the role of natural convection but largely aids the overall heat-transfer process during solidification. The heat-discharge rate of twisted-fin configuration is increased by ∼14 and ∼55% compared to straight fin and no fin configurations—leading to a reduction in the solidification duration by ∼13 and ∼35%, respectively. The solidification front at various times has also been assessed through a detailed parametric study over the fin height, fin pitch number, and fin thickness. Over the range of values assumed, the fin height is the most dominant parameter – increasing the heat-retrieval rate from 10.0 to 11.4 W and decreasing the discharge time from above 3600 to 2880 s by varying the fin height from 2.5 to 7.5 mm.

Keywords: latent heat, energy storage, solidification, enhancement, twisted fins

Nomenclature

A_m: Mushy zone constant (-)
C_p: Specific heat-transfer coefficient ($J\,kg^{-1}\,K^{-1}$)
g: Gravity ($m\,s^{-2}$)
k: Thermal conductivity ($W\,m^{-1}\,K^{-1}$)
L_f: Latent heat ($J\,kg^{-1}$)
P: Pressure (Pa)
t_m: Melting/solidification time (s)
T: Temperature (K)
$\vec{V}$: Velocity ($m\,s^{-1}$)
$\dot{Q}$: Heat-discharging rate (W)

Greek symbols

β: Expansion coefficient (K^{-1})
λ: Liquid fraction (-)
μ: Viscosity ($kg\,m^{-1}\,s^{-1}$)
ρ: PCM Density ($kg\,m^{-3}$)
ΔH: PCM enthalpy of fusion ($J\,kg^{-1}$)
h: PCM specific enthalpy ($J\,kg^{-1}$)

Subscripts

S: Solid state of PCM
L: liquid state of PCM

1. Introduction

According to the recent report by International Energy Agency (IEA), fossil-based energy resources including oil, coal, and natural gas contribute to 81.3% of the total primary energy consumption in 2019—each accounting for 30.9, 26.8, and 23.2%, respectively (IEA, 2021). To meet the greenhouse gas emissions reduction targets set by the Paris Agreement, it is imperative to identify a sustainable and carbon-free replacement for fossil fuels (Zhang *et al.*, 2016). The traditionally fossil-powered systems can be retrofitted such that they consume renewable energy as the driving source (Li & Wang, 2022). As such, there is a significant shift away from fossil fuels toward the development of renewable energy technologies (Yan *et al.*, 2022). Among renewable resources, solar energy has received a significant research impetus as an alternative source of energy (Shahsavari & Akbari, 2018; He *et al.*, 2022; Wang *et al.*,

Received: April 19, 2022. **Revised:** August 24, 2022. **Accepted:** August 26, 2022

2022). To accelerate the uptake of solar energy, the main challenge to overcome is the time delay or mismatch between energy supply and demand as a result of daily/hourly fluctuations of solar resources caused by the day/night cycle as well as cloud cover (Shahsavar *et al.*, 2013, 2022; Ye, 2016, 2017; Wang & Tan, 2019; Ye *et al.*, 2019; Shi *et al.*, 2022).

To accommodate the solar fluctuations and ensure an uninterrupted supply of energy, thermal energy storage (TES) technology enables the storage of surplus thermal energy which can then be used for downstream applications during high-demand periods (Chavan *et al.*, 2022; Wu *et al.*, 2022). TES systems are categorized into latent heat TES (LHTES), sensible heat TES (SHTES), and thermochemical TES (TCTES) (Reddy *et al.*, 2018). Among these technologies, SHTES requires a larger vessel relative to other options. TCTES, although offering high-energy storage density, is at an early stage of research (Ibrahim *et al.*, 2017). It has been argued that LHTES is a promising trajectory with a relatively low cost, a high storage density, and the ability to store energy at a constant or nearly constant temperature corresponding to the phase-transition temperature of phase change materials (PCMs, Sharma *et al.*, 2009; Mahmood, 2019). PCMs are classified into organic, inorganic, and eutectics. Further information about the melting/freezing temperatures of the PCMs can be found in the following references (Farid *et al.*, 2004; Agyenim *et al.*, 2010). Low thermal conductivity is the main undesirable feature of most PCMs excluding the metallic-based PCMs—affecting the response rates during charging and discharging cycles, which eventually lowers the energy performance of TES (Wang *et al.*, 2018; Mahdi *et al.*, 2019). To tackle this, several approaches have been proposed in the literature including geometry modification (Shahsavar *et al.*, 2019a, b), fin position (Jmal & Baccar, 2018; Mahdi *et al.*, 2018; Luo *et al.*, 2022), nanoparticle addition (Mahdi & Nsofor, 2016, 2017a, 2018; Yan *et al.*, 2019), nano-encapsulation (Ghalambaz *et al.*, 2019), magnetic field (Ghalambaz *et al.*, 2020), and use of metal foams (Mahdi & Nsofor, 2017b; Ghalambaz & Zhang, 2020). There is an increasing interest in the use of fins in LHTES systems—as a means of improving the charging/discharging response—due to the low-fabrication cost, easy installation, and high heat-transfer-enhancement rate (Agyenim *et al.*, 2009; Hosseinzadeh *et al.*, 2021). In this regard, the main emphasis has been placed on the configurations of fins as well as the optimization of their geometric parameters (Gao *et al.*, 2020; Wang *et al.*, 2022). The most conventional shape of fins employed in LHTES systems includes longitudinal and annular fins.

Focusing on longitudinal fins, Nóbrega *et al.* (2020) performed experiments to assess the solidification performance of PCM around finned tubes. Increasing the fin numbers and fin width was associated with a reduction in the time to achieve complete solidification. Following this work, the authors developed a correlation for predicting the interface position, interface velocity, PCM solidified mass and solidification time as a function of tube wall temperature, fin numbers, and fin width and time (Nóbrega *et al.*, 2019). Patel and Rathod (2019) investigated the charging and discharging processes of a triple-tube heat exchanger with different arrangements of longitudinal fins. A case with internal-external fins reduced the melting and solidification time by 60 and 57%, respectively. Abdulateef *et al.* (2017, 2018) compared the solidification and melting processes of PCM in a triple-tube heat exchanger with longitudinal and triangular fins in various configurations. The external triangular finned tube achieved the lowest solidification time of 630 min—which was 6 and 30% lower than internal and internal-external triangular fin configurations, respectively. In a recent study by Huang and Yao (2021), the authors proposed trapezoidal longitudinal fins distributed by the Fibonacci sequence as a means of enhancing the solidification performance of an LHTES unit. They were able to shorten the solidification time by 45.28% compared to the traditional quadrilateral fin. Hassan *et al.* (2020) conducted experiments to compare the thermal performance of a shell-and-tube LHTES system with longitudinal and annular fin geometries. The saving in the charging time in the case of annular fins was much larger than longitudinal fins—reduced by ∼70 and ∼55% compared to the case with no fins.

The results by Hassan *et al.* (2020) were part of a much larger initiative for improving the thermal performance of a storage system using annular fins. With this picture in mind, a great deal of effort has been dedicated to the optimization of annular-fin geometrical parameters. Erek *et al.* (2005) were among the first who conducted experimental and numerical investigations of the solidification performance of a shell-and-tube LHTES with annular fins. The maximum 20% decrease in the solidification time was achieved by either decreasing the fin space or increasing the fin height. In 2013, AL-Abidi *et al.* (2013b) studied a triple-tube heat exchanger with the presence of annular fins to improve the charging and discharging period of PCM. The number of fins was the most dominant factor to achieve complete solidification in a shorter time compared with the fin length and thickness. In a follow-up numerical study by Jamal and Baccar (2015), the authors found that there is insignificant benefit in the solidification process by increasing the fin numbers beyond a certain point due to the PCM liquid fraction effect on the thermo-convective development of the flow. In the same line of thinking, Yang *et al.* (2017) focused on optimizing the fin number, thickness, and interval to maximize the heat transfer in a shell-and-tube LHTES unit fitted with annular fins. In a more recent study, Tiari *et al.* (2021) considered a constant fin volume with varying length, thickness, and number in an LHTES system to assess the charging and discharge processes. It was found that doubling the fin numbers—with uniform length—while halving the fin thickness decreased the discharging time by 79.2%. Geometrical optimization of annularly finned LHTES units has been reported in the following papers (Pu *et al.*, 2020; Yang *et al.*, 2020; Elmaazouzi *et al.*, 2021).

According to the above-mentioned literature, there are several studies dealing with the application of longitudinal and annular fins to enhance the charging and discharging rates of the PCM. The major significant observations from these studies are: (i) the melting and solidification times can be significantly reduced through optimizing the fin geometry (i.e., height, thickness, and number), (ii) in both configurations, the heat-transfer enhancement in horizontally oriented TES systems attract more attention than that using vertically oriented TES systems, and (iii) compared to longitudinal and annular as conventional fin configurations, tree-like (Hosseinzadeh *et al.*, 2019; Huang & Liu, 2021), ladder-shaped (Liu *et al.*, 2022), and twisted (or spiral) (Youssef *et al.*, 2018; Arasteh *et al.*, 2021; Ghalambaz *et al.*, 2021a, b; Lu *et al.*, 2021; Mashayekhi *et al.*, 2022a, b) fins have been suggested in the literature due to their better enhancement capacity per system's volume (Arasteh *et al.*, 2021; Mehta *et al.*, 2021; Mashayekhi *et al.*, 2022a). Among the proposed alternatives, twisted fins are the promising candidate to generate swirl flow in the liquid phase of PCM and, as a result, enhance flow mixing and disrupt the development of the boundary layer. It should be noted that the contribution of convection heat-transfer mechanism to the overall heat-transmission process is intensified by increasing the flow mixing intensity. However, the use of twisted fins in LHTES systems is less understood in the literature.

In recent studies by Ghalambaz *et al.* (2021a, b), the authors employed twisted-fin arrays to improve the charging rate of the PCM in a shell-and-tube heat exchanger. They were able to improve the melting time by 42% in the case of a double-tube heat exchanger (Ghalambaz *et al.*, 2021a) and by 18% in the case of a triple-tube heat exchanger (Ghalambaz *et al.*, 2021b) compared to the straight longitudinal fins using similar geometrical parameters. The authors, however, did not analyze the discharging performance of either double-tube or triple-tube LHTES systems with the presence of twisted fins nor did they discuss the optimal fin parameters to achieve an optimal discharging rate of the LHTES system.

Reviewing the preceding papers reveals that there have been ongoing attempts to enhance the thermal performance of PCMs in the LHTES. The main focus of previous studies lies in optimizing longitudinal or annular fin parameters for LHTES systems. The importance of twisted-fin arrays on the thermal behavior of PCMs during the solidification process has not yet been thoroughly analyzed in the literature. As such, more insights are yet to be gained especially with regard to fin parameters optimization. To the best of the authors' knowledge, this is the first numerical study examining the solidification performance of a shell-and-tube LHTES unit with twisted-fin arrays. The solidification front at various times is compared with the reference cases being no fin and straight fin configurations. This is followed by a detailed parametric study of the fin parameters—including the fin height, fin pitch number, and fin thickness—to maximize the thermal performance of the LHTES unit. The emerging trends in accelerating the uptake of solar energy as a clean and sustainable energy production pathway require studies that point toward the development of fast-responsive PCMs during charge-discharge cycles.

2. Problem Description

A double-pipe heat storage system equipped with twisted fins is studied during the solidification process. The length of the heat storage unit is 250 mm while the inner and outer tube diameters are 20 and 40 mm, respectively. The system is compared with a double-pipe system with uniform fins and without fins. Figure 1a shows the schematic of the system with twisted fins. Four twisted fins are attached to the inner tube. The PCM is located in the outer pipe while the heat-transfer fluid (HTF) is passed through the inner tube. The boundary conditions and gravity direction are also displayed in Fig. 1. The system is placed vertically to better present the proposed geometry, as shown in Fig. 1b. The system with uniform straight fins is also displayed in Fig. 1c.

Water with a uniform inlet temperature of 15°C and Reynolds number of 1000 is passed through the tube to gain heat from the PCM. The outer tube and the sides of the heat exchanger in contact with the PCM are considered insulated to eliminate the effect of heat loss. A pressure outlet boundary condition is assumed for the outlet surface of the central tube, and a no-slip boundary condition is considered for all the walls. Effects of different geometrical parameters of the twisted fins including the height and thickness of the fins as well as the pitch number of twisted fins are examined to obtain the optimum configuration. Table 1 shows the properties of the RT35 PCM.

3. Mathematical Modeling

The enthalpy–porosity approach is incorporated to estimate the phase change process (Sardari *et al.*, 2020). The natural convection flow of the melted PCM occurring due to the buoyancy force

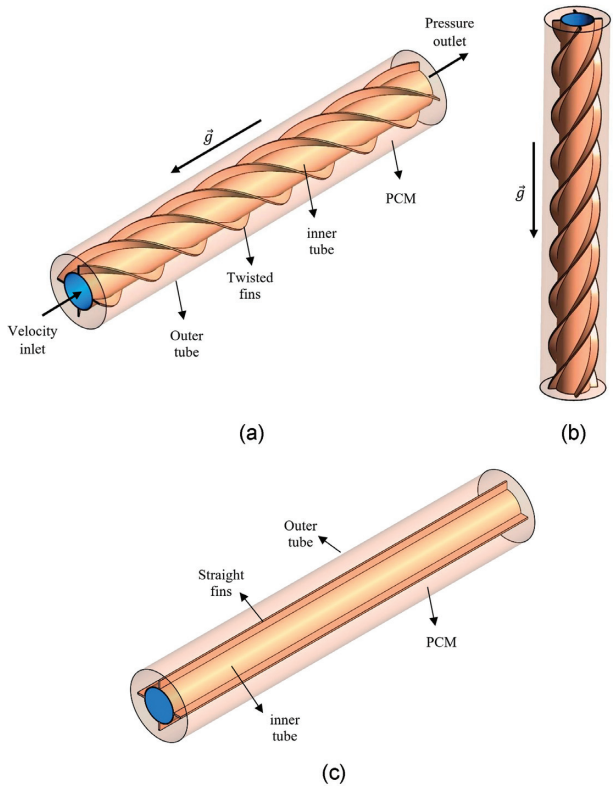

Figure 1: Schematic of the system with (a) twisted fins including boundary conditions, (b) twisted fins in vertical placement, and (c) straight fins in vertical placement.

is transient and laminar. The Boussinesq approximation is used to predict the temperature-based density variation. Viscous dissipation is also neglected due to the low velocities of the molten PCM. Considering the above assumptions, the governing equations are as follows (Shahsavar *et al.*, 2021):

$$\frac{\partial \rho}{\partial t} + \nabla.\rho\vec{V} = 0, \tag{1}$$

$$\rho\frac{\partial \vec{V}}{\partial t} + \rho\left(\vec{V}.\nabla\right)\vec{V} = -\nabla P + \mu\left(\nabla^2\vec{V}\right) - A_m\frac{(1-\lambda)^2}{\lambda^3+0.001}\vec{V} - \rho_{ref}\beta\left(T-T_{ref}\right)\vec{g}, \tag{2}$$

$$\frac{\rho C_p \partial T}{\partial t} + \nabla\left(\rho C_p\vec{V}T\right) = -\left[\frac{\partial \rho\lambda L_f}{\partial t} + \nabla\left(\rho\vec{V}\lambda L_f\right)\right] + \nabla\left(k\nabla T\right). \tag{3}$$

The momentum sink for the phase change in the mushy zone is represented as the third term on the right-hand side of Equation (2). The volume expansion due to change in the PCM from solid to liquid state is neglected in this research, and A_m was considered 10^{-5} (Fadl & Eames, 2019). For the water flow simulation in the inner tube, similar governing equations are employed, ignoring the body forces and phase change equation. λ is introduced as (Al-Abidi *et al.*, 2013a)

$$\lambda = \frac{\Delta H}{L_f} = \left\{0 \quad if T < T_s \frac{(T-T_s)}{(T_L-T_s)} \quad if T_s < T < T_L\ 1 \quad if T > T_L\right\}. \tag{4}$$

A detailed description of the mathematical model can be found in the authors' previous work (Sardari *et al.*, 2020; Shahsavar *et al.*, 2021). The total enthalpy (H) is expressed as:

$$H = h_{ref} + \int_{T_{ref}}^{T} C_p dT + \lambda L_f, \tag{5}$$

where h_{ref} denotes the specific enthalpy at the standard temperature of 298 K.

Table 1: Characteristic values of RT35 PCM (Rubitherm, 2020).

Property	μ (Ns m^{-2})	β (K^{-1})	C_p (kJ kg^{-1} K^{-1})	K (W m^{-1} K^{-1})	(kg m^{-3})	L_f (kJ kg^{-1})	T_L (°C)	T_s (°C)
Values	0.023	0.0006	2.0	0.2	815	170	35	29

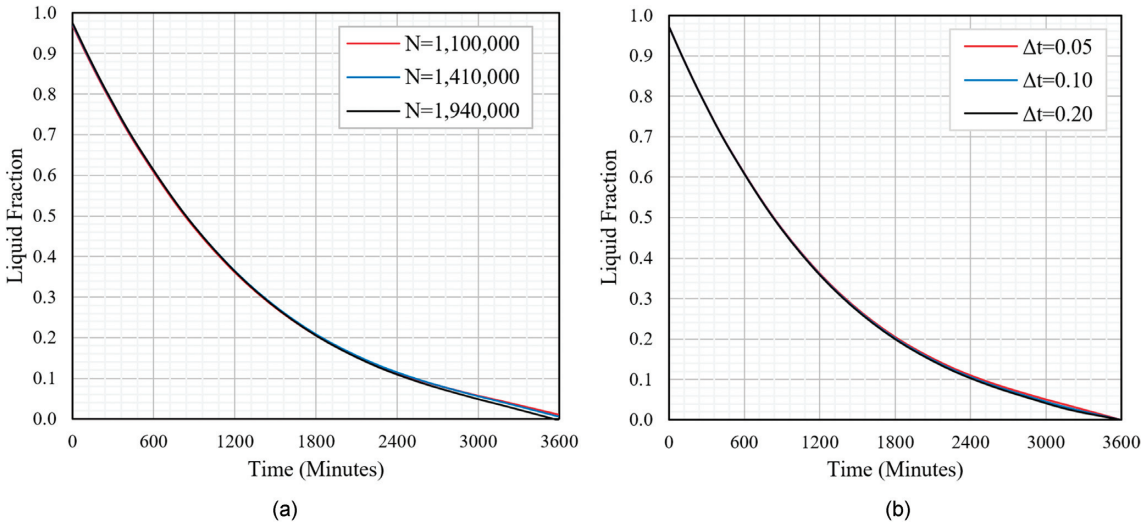

Figure 2: Independency test results for (a) the mesh density and (b) the timestep size.

The solidification or discharging rate $\dot{Q}$ is introduced as (Xu *et al.*, 2017)

$$\dot{Q} = \frac{Q}{t_s} = \frac{m\left(\int_S C_p dT + L_f + \int_L C_p dT\right)}{t_s}, \quad (6)$$

where t_s is the solidification time, and m is the mass of PCM.

4. Numerical Modeling and Validation

The simulation is performed in ANSYS-Fluent software employing the QUICK scheme for the diffusion fluxes and convection and PRESTO scheme for the pressure correction equation. The convergence criteria of 10^{-6} is also assumed. Different mesh elements and time-step sizes are evaluated so that the results are unconditional to grid density and time step. Grids with N = 1100 000, 1410 000, and 1940 000 cell elements are generated for the grid independence analysis shown in Fig. 2a. The mesh with the cell number of 1410 000 is selected since the results are identical to those of 1940 000 meshes. As also illustrated in Fig. 2b, three different timestep sizes of 0.05, 0.10, and 0.20 s are examined for the selected grid. The results show that the variations of liquid fraction for all the studied sizes of time step are similar and, as a result, the time step size of 0.20 s is selected to reduce the computational time.

To validate the proposed numerical model during the solidification, these results are compared with Al-Abidi *et al.* experimental investigation (Al-Abidi *et al.*, 2014). They examined the temperature distribution of PCM in a triple-pipe PCM-based heat exchanger which was equipped with fins in the longitudinal direction. They employed 15 thermocouples to measure the temperature in different locations. Figure 3 shows the geometry studied by Al-Abidi *et al.* (2014) as well as the locations of thermocouples which are used as predefined points in the numerical model to capture the temperature to validate the model.

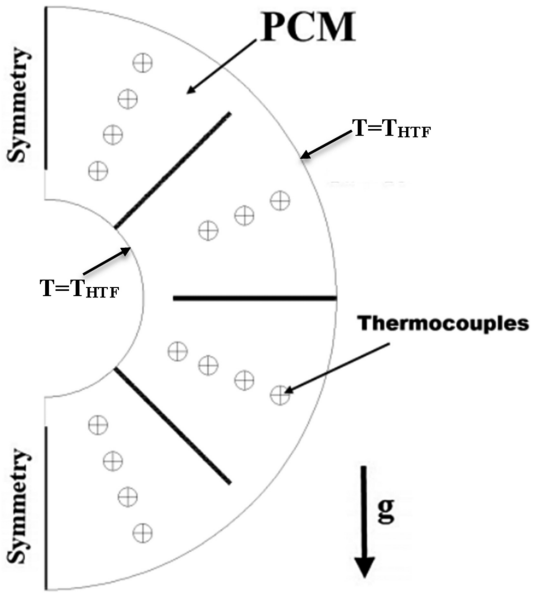

Figure 3: A schematic of the simulated geometry for the model verification proposed in the study of Al-Abidi *et al.* (2014).

As illustrated in Fig. 4 which shows the mean temperature variation, there is a good agreement between this study and those reported by Al-Abidi *et al.* (2014). This indicates that this model accurately predicts the solidification process relative to the experimental data.

5. Results and Discussion

Simulations have been performed to investigate the potential of expediting the energy-retrieval rate from the PCM during the so-

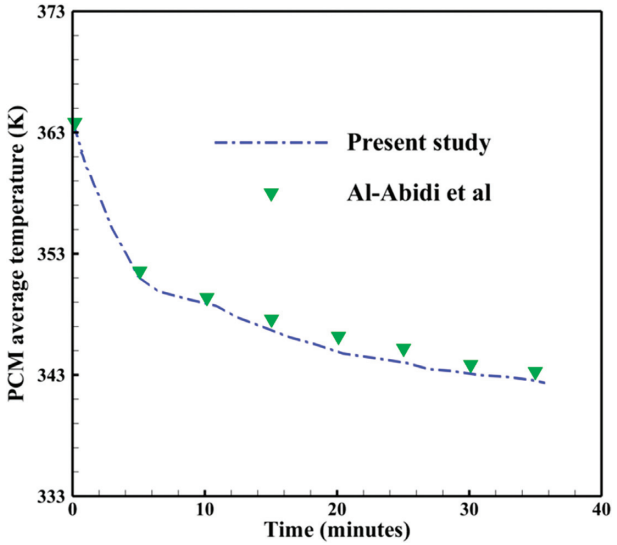

Figure 4: Benchmarking of the solver with the experimental results reported by Al-Abidi *et al.* (2014).

lidification mode via twisted fins in a vertical double-tube containment system. The research mainly explores three cases: no fins, straight fins, and twisted fins. The total mass of PCM is maintained equal to 0.335 kg in all the proposed cases to allow for making meaningful comparisons in terms of the storage performance indexes. Three essential indexes were adopted for performance assessment: solidifying-front evolution contours, isotherm distribution contours, and timewise solidifying-front profiles. In all the considered cases, it is assumed that the scenario to reach the whole solidification status is started when the PCM at starting temperature ($T_{int} = 50°C$ K) is designated to be higher than the PCM liquidus temperature ($T_l = 35$ K) to make sure that the PCM solidification was starting from a fully liquid phase. Meanwhile, the HTF (water) is circulating at a lower temperature (i.e., 323 K) to achieve the required cooling load. This in turn helps the solidification of PCM next to the thermally active partitions in the domain, so that the PCM molecules closest to the cooling partitions provoke the completion of solidification earlier than the other PCM parts. From the obtained results, it is evident that the inclusion of twisted or straight fins facilitates quicker heat-retrieval rates from the PCM by circulating HTF on the shell side—resulting in an improved energy retrieval process throughout the whole TES unit.

5.1. Impact of applying twisted fins

A parametric analysis has been conducted to evaluate the performance of twisted fins during the solidification process as compared to other cases being no fins and straight fins. Figure 5 shows the liquid-fraction contours, including the solidifying fronts (in light green) for the cases of no fins, straight fins, and twisted fins at five unique vertical positions during six solidification durations of 600, 1200, 1800, 2400, 3000, and 3600 s. In the early duration (i.e., 600 s), solidifying fronts that are marked in light green resemble homogeneous circles, equivalent in the vertical direction in the case of no fins. Adding fins, particularly twisted fins, results in an increase in the size of solidifying layers (blue areas) between and around the fin zones (see Fig. 5). Due to the fact that only thin solid layers could be formed during this time duration, the fronts are rarely observed to be moving apart during this duration. With passing to the second duration (i.e., 1200 s), the shapes of solidifying fronts become increasingly deformed, particularly in cases involving fins. This is because of heat-removal rates at the cooling walls, which continue to rise as time further progresses. The same figure shows that the size of the solidifying layers (blue zones) seems to be expanding progressively toward the bottom at the third duration of the 1800 s. The reason is that convection plays a vital role in the upper half of the domain than it does in the bottom half. Twisted fins, on the other hand, profit from the fact that it provides better heat diffusion to the PCM parts far away from the thermally-active walls, so the solidifying layers expand in size more quickly during the later duration (i.e., 2400 s). By increasing the distortion of the solidifying front in the presence of twisted fins compared to straight fins, natural convection plays a greater role. This is because the flow-resisting forces produced by twisted fins are less influenced as they have their own flow-aiding structure, which makes them more favorable than straight fins in promoting heat transfer by natural convection. During the last durations (i.e., 3000 and 3600 s), the liquid-fraction field turns entirely into a solid phase in the bottom section of the domain owing to the little function of convection in this region but is delayed in the upper section due to the greater local convection. In conclusion, when twisted fins are applied while retaining a constant total mass of PCM, solidifying fronts move more rapidly than when straight fins are applied under the same thermofluidic conditions.

The isotherm progression for the three different cases investigated in this section (i.e., no fins, straight fins, and twisted fins) throughout the six durations of solidification (600, 1200, 1800, 2400, 3000, and 3600 s) is demonstrated in Fig. 6. At first glance, it seems that the low-temperature isotherms around 300 K (the blue regions) appear to be the leading band throughout the whole cavity in all the cases investigated at the early durations (600–1800 s). This is attributed to the major portion of PCM being liquid throughout these durations. As such, there is little influence of solidification on the isotherm distribution, and the isotherms between and in close proximity to the fin ligaments seem to be almost identical in their behavior and appearance. The isotherms with higher temperatures exceeding 305 K (turquoise regions) begin to gradually diminish somewhat across the domain, especially in the cases with fins during the subsequent durations (2400–3000 s). During this duration, the cooling impact of the HTF on the PCM solidifying behavior becomes more effective, causing the solidifying layer to become larger and eventually occupy the whole domain. Furthermore, the presence of fins contributes to improving the heat release from the PCM towards the HTF as it allows for more efficient communication between the farther PCM layers from the thermally active walls and the HTF. In contrast to the base case with no fins, there seems to be a greater shrinkage of isotherms at high temperatures (the red zone) in the cases with fins. This is especially true while heading downward. The implications of this include that convection currents have little influence in the case of fins, especially in the upper region of the domain as compared to conduction heat transfer. The isotherms seem to be more uniform and persistent in their shape and behavior throughout the last duration (i.e., 3600 s). However, in cases with fins, the isotherms appear to be less uniform and inconsistent during the preceding durations, especially in the bottom region of the domain. Because of the predominant role of heat conduction in this location, the solidification process is completed sooner relative to other locations. Indeed, the presence of twisted fins contributes to the dominating role of heat conduction by virtue of their curved shapes, which restricts the role of natural convection but largely aids the overall heat-transfer process during solidification.

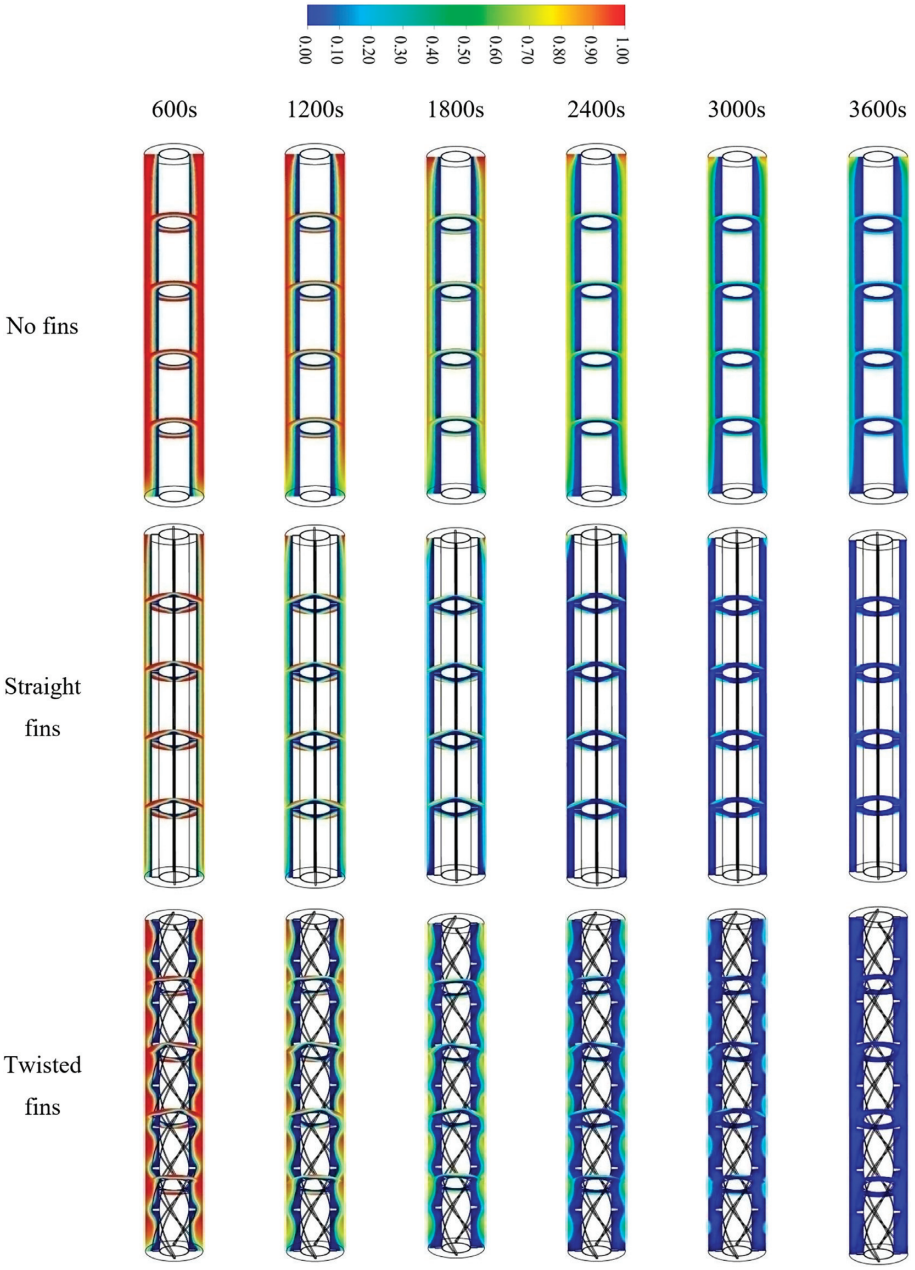

Figure 5: The contours of liquid-fraction evolution for different arrangements of no fins, straight fins, and twisted fins at distinct durations of the solidification process.

The temporal behavior of the PCM liquid fraction and the average PCM temperature have also been analyzed to better understand the prospects of solidification intensification by employing twisted fins. Figure 7 depicts the liquid fraction as a function of time during solidification for the three different configurations. Among the three cases investigated, the twisted fin arrangement has the most potential to intensify the solidification progression. The figure also indicates that the twisted fins provide a more favorable boost to the PCM solidifying rate than other cases under the same PCM mass constraints. According to the data from Table 2, the solidification time can be reduced from 5686 to 3644 s by employing the twisted fins compared to the base case of no fins—which is about a 36% time-saving. In addition, the twisted fins have the potential to lower the solidification time by about 13% compared to the case of straight fins. In terms of heat-removal rate, the twisted fins can remove 11.28 W of heat from PCM, while this value is 9.91 and 7.28 W in straight fins and no fins cases, respectively. These data imply that the heat-discharge rate increases by about 55 and 36% for twisted fins and straight fins as compared to the baseline case of no fins, respectively.

Figure 8 displays the PCM temperature variation during solidification mode for the three configurations. As seen in this figure, the minimum temperature of PCM is attained in the case of twisted fins within a shorter time as compared to other cases. This indicates that the time required to achieve the minimum solidification temperature is significantly reduced by using twisted fins in place of straight fins or no fins. The reason is that the employment of twisted fins typically provides faster rates of heat transport from the PCM towards the cooling walls—resulting in earlier termination of the PCM solidification process.

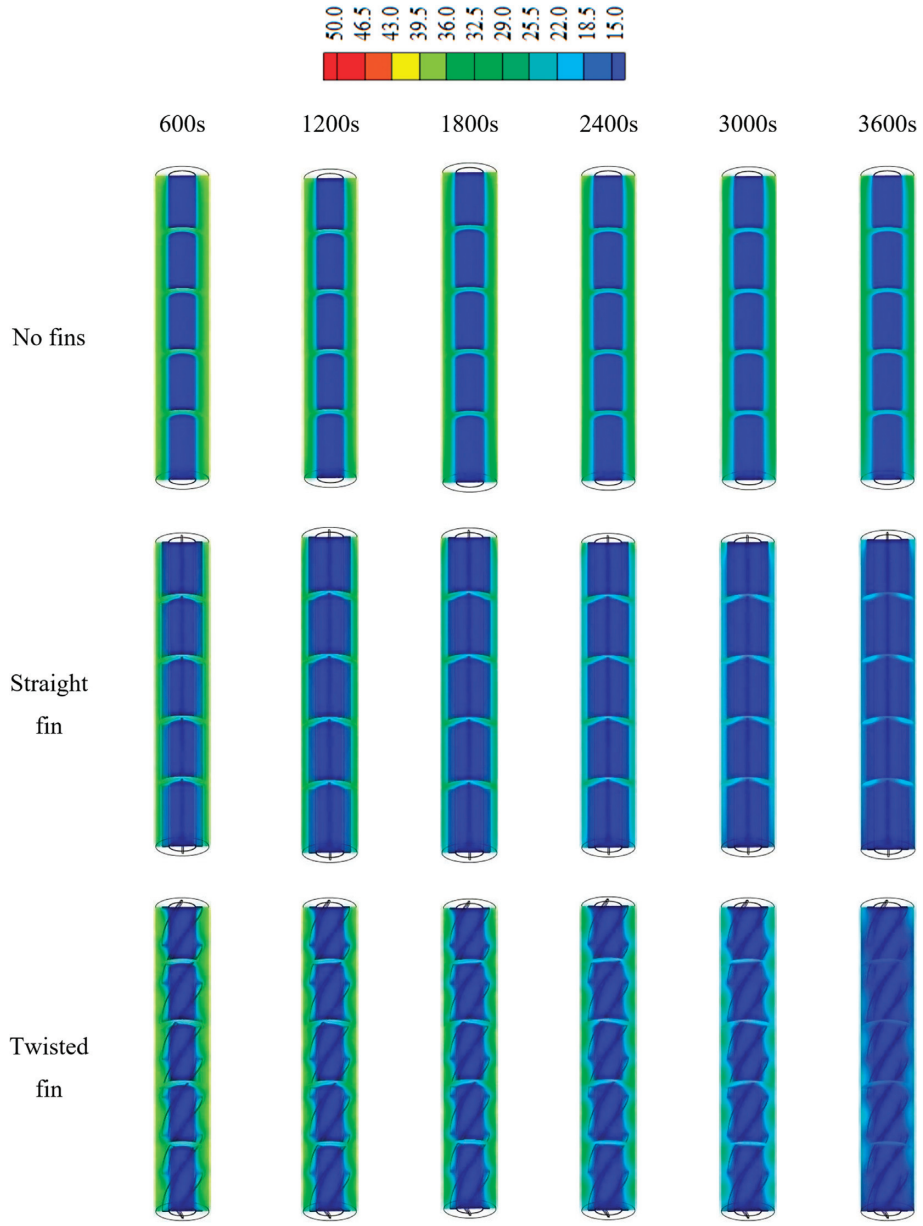

Figure 6. The contours of temperature distribution for different patterns of no fins, straight fins, and twisted fins at distinct durations of the solidification process.

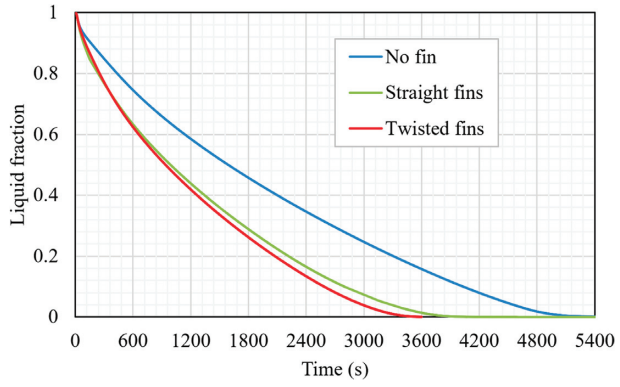

Figure 7: The temporal profiles of PCM liquid-fraction for three different cases: no fins, straight fins, and twisted fins.

Table 2: The solidification time and heat-retrieval rates for three different cases: no fins, straight fins, and twisted fins.

Fin type	Solidification time (s)	Heat-retrieval rate during solidification time (W)
No fins	5686	7.28
Straight fins	4189	9.91
Twisted fins	3644	11.28

5.2. Impact of twisted-fin height

Figure 9 shows the liquid-fraction contours for the cases of twisted fins with a fin height of 2.5 and 7.5 mm during six solidification durations of 600, 1200, 1800, 2400, 3000, and 3600 s. As the fin height rises, there is a visible distortion in the solidifying front's shape due to the greater heat retrieval from the PCM. As seen in this figure, the size of the solidifying layers (blue zones)

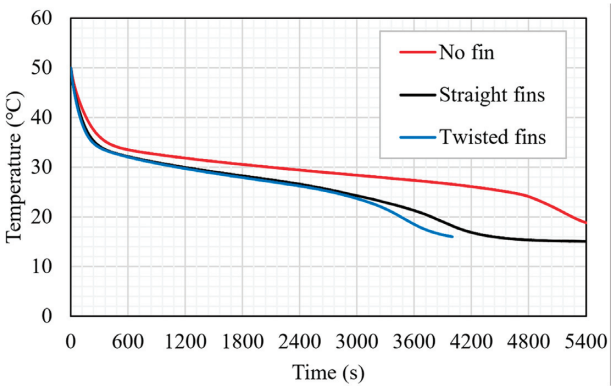

Figure 8: The temporal profiles of the average PCM temperature for three different cases: no fins, straight fins, and twisted fins.

seems to steadily rise towards the bottom at the initial durations of 600–1800 s. The major portion of the TES unit exhibits a quicker completion of solidification near and between the fin ligaments at a fin height of 7.5 mm due to an improvement in the heat diffusion in these regions. Due to the detrimental effect of fins on the buoyant flow of liquid PCMs in these regions, convection is projected to play a minimal role in the heat-transfer process. By improving the height of twisted fins from 2.5 to 7.5 mm at the later durations of 1800–2400 s, the twisting fins promote heat diffusion in both the vertical and angular directions, giving the solidifying front the ability to travel faster through the whole PCM domain. Therefore, the solidification process is terminated earlier (i.e., 3000 s) at the fin height of 7.5 mm. In this case, the larger surface area of twisted fins contributes to enhanced heat transport by conduction between the different components of the PCM. Meanwhile, this limits the contribution of natural convection due to the higher generated flow-resistant forces as the fin height increases.

Figure 10 compares the temperature fields for the cases of twisted fins with a fin height of 2.5 and 7.5 mm over six different durations. A little change in the distribution of isotherms may be seen as the fin height increases during the early durations (600–1800 s), indicating that a significant portion of PCM has not yet solidified and hence cannot be clearly identified. However, as time progresses to 1800–2400 s, the size of the solidifying layer grows as a result of the increased heat removal from the PCM that occurs as a result of the presence of a greater fin height. According to the results, the impact of increasing the fin height is more visible as the solidification time further advances. Latent TES units during solidification are often characterized by the predominance of gravity over buoyancy in terms of the flow of liquid PCM inside them. The reason is that the higher density of solid PCM compared to liquid negatively affects natural convection, thus decreasing the rate of solidification in the top regions. Due to the downward direction of gravity, cooler liquid PCM layers that appear around the fin ligaments move to the lower regions, causing more heat removal from solid PCM to the liquid PCM and thus increasing the rate of so-

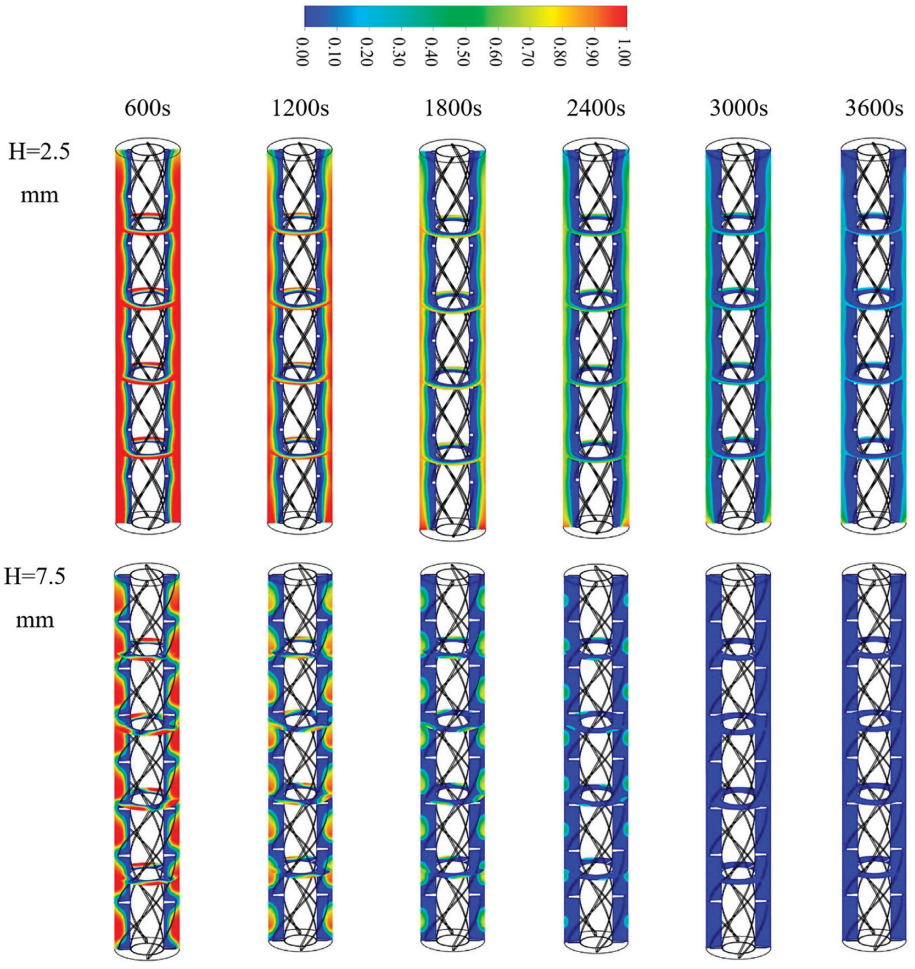

Figure 9: Liquid-fraction contours for fin heights (H = 2.5 and 7.5 mm) over different solidification durations.

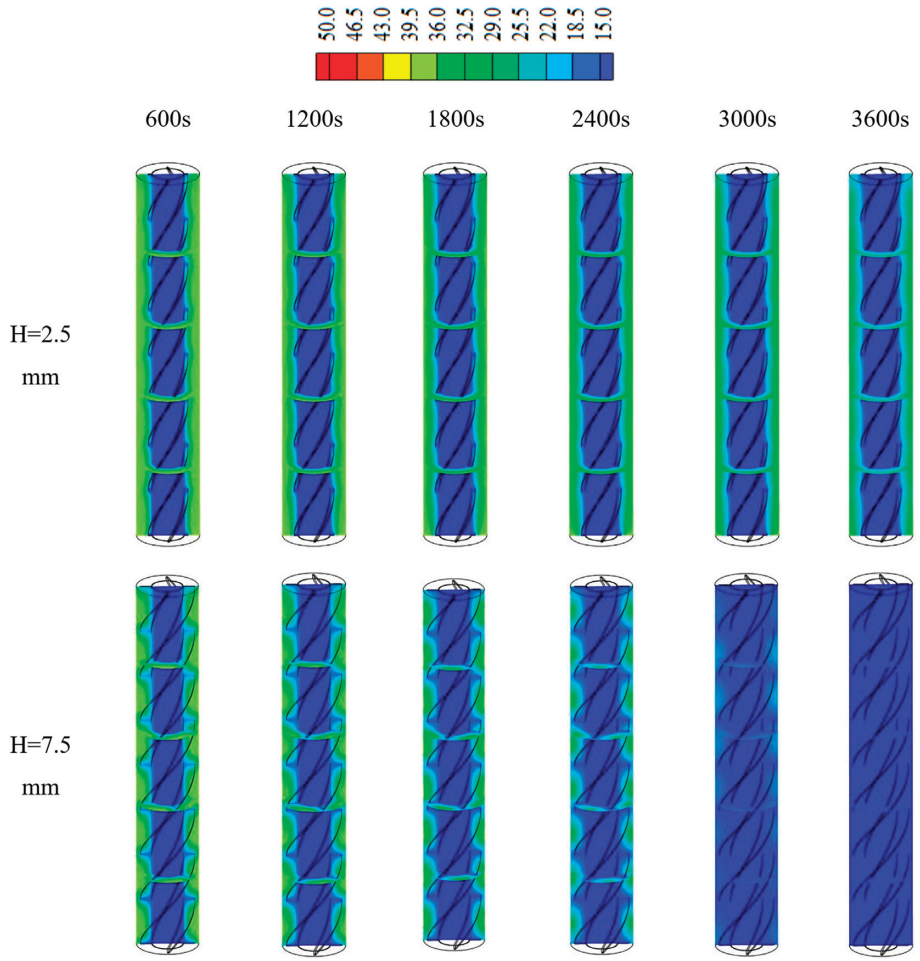

Figure 10: Temperature distribution contours for fin heights (H = 2.5 and 7.5 mm) over different solidification durations.

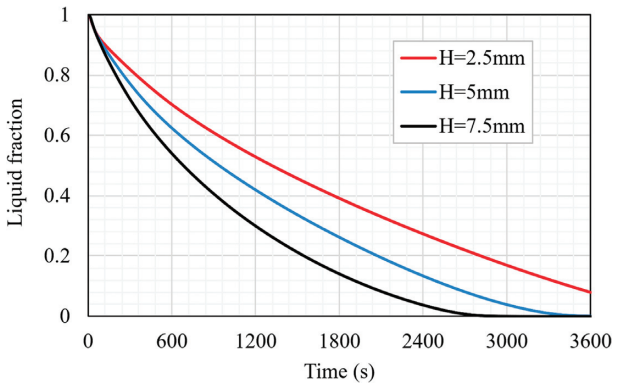

Figure 11: The temporal profiles of PCM liquid fraction for three different cases of twisted-fin height.

lidification in the lower portions of the domain. This results in a greater temperature differential across the lower portions of the domain with an earlier solidification termination, as evidenced in Fig. 9, by comparing isotherms of the 7.5 mm fin height to those of 2.5 mm at 3000 s.

Figure 11 illustrates the temporal variation in the liquid-fraction profile for various fin heights. As seen in this figure, the PCM with a greater fin height takes less time to fully solidify (less than 3000 s) than that for the other cases. This is attributed to

Table 3: The heat-retrieval rates during 3600 s of solidification for three different cases of twisted-fin height.

Fin height (H)	Heat-retrieval rate
2.5 mm	9.98 W
5.0 mm	10.70 W
7.5 mm	11.37 W

the fact that by increasing the fin height, the volume occupied by the fins inside the PCM domain increases—resulting in a larger heat-exchange area of twisted fins with a lower amount of PCM that can be contained by the TES unit. Consequently, the case of twisted fins with a height of 7.5 mm is the best case among the considered cases. The data from Table 3 shows that the highest heat-retrieval rate is due to both the effects of the heat-exchange area and the amount of PCM in charge. Twisted fins with 7.5 mm fin height are capable of removing 11.37 W of heat from PCM, whereas other cases of fin heights being 5.0 and 2.5 mm are capable of removing 10.70 and 9.98 W, respectively. This indicates that the heat-discharge rate rises by about 7.2 and 13.8% when twisted fins with a height of 7.5 mm are used compared to 5.0 and 2.5 mm cases.

Figure 12 displays the PCM temperature variation of twisted fins during solidification mode for the three fin heights. Increasing the height of twisted fins does not have a significant effect during

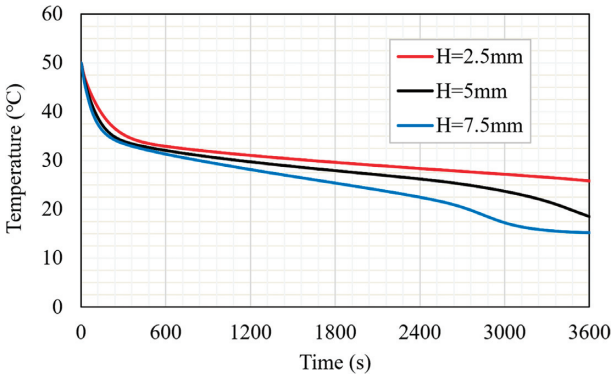

Figure 12: The temporal profiles of the average PCM temperature for different cases of twisted-fin height.

the early stages of solidification (i.e., 600–1200 s). Although it is not immediately visible at first glance, the difference in the average temperature becomes more evident as time progresses when the fin height is increased from 2.5 to 5.0 m and 7.5 mm. The average temperature can be reduced to its lowest possible value in a shorter time by increasing the fin height so that quicker heat-discharge rates from the PCM can be achieved—leading to faster solidification.

5.3. Impact of fin pitch number

Figure 13 shows the liquid-fraction contours for the effect of pitch number in the case of twisted fins during six solidification durations of 600, 1200, 1800, 2400, 3000, and 3600 s. In the early duration of 600–1200 s, the solidifying fronts (light green) virtually took the form of waving lines parallel to the fin walls. As seen in this figure, increasing the pitch number of fins improves the solidifying layers (blue zones) during the same time. The twisted fins showed significant displacement in terms of the solidifying front during the subsequent period of 1800–2400 s). The difference between the two cases of fin pitch in terms of the amount of the solidified PCM is more noticeable as compared to that in the preceding period. The more closely spaced fin by increasing the fin pitch provides a larger heat diffusion in a specific volume so that faster rates of solidification are achieved. This behavior is particularly obvious during the final duration (i.e., 3000–3600 s). Due to the higher heat diffusion by twisted fins at a pitch number of 3, the PCM takes a shorter time to solidify due to the larger amount of solidified PCM generated near and around the fin walls.

Figure 14 compares the isotherm distributions for the case of twisted fins with two different fin pitches. At the initial duration of 600–1200 s, the isotherms grouped as condensed lines parallel to the fin walls. This is because pure conduction dominates heat transport during this period. As such, the heat removal from liquid PCM via the circulating HTF is governed by conduction, and the change of fin pitch has no major influence on isotherm

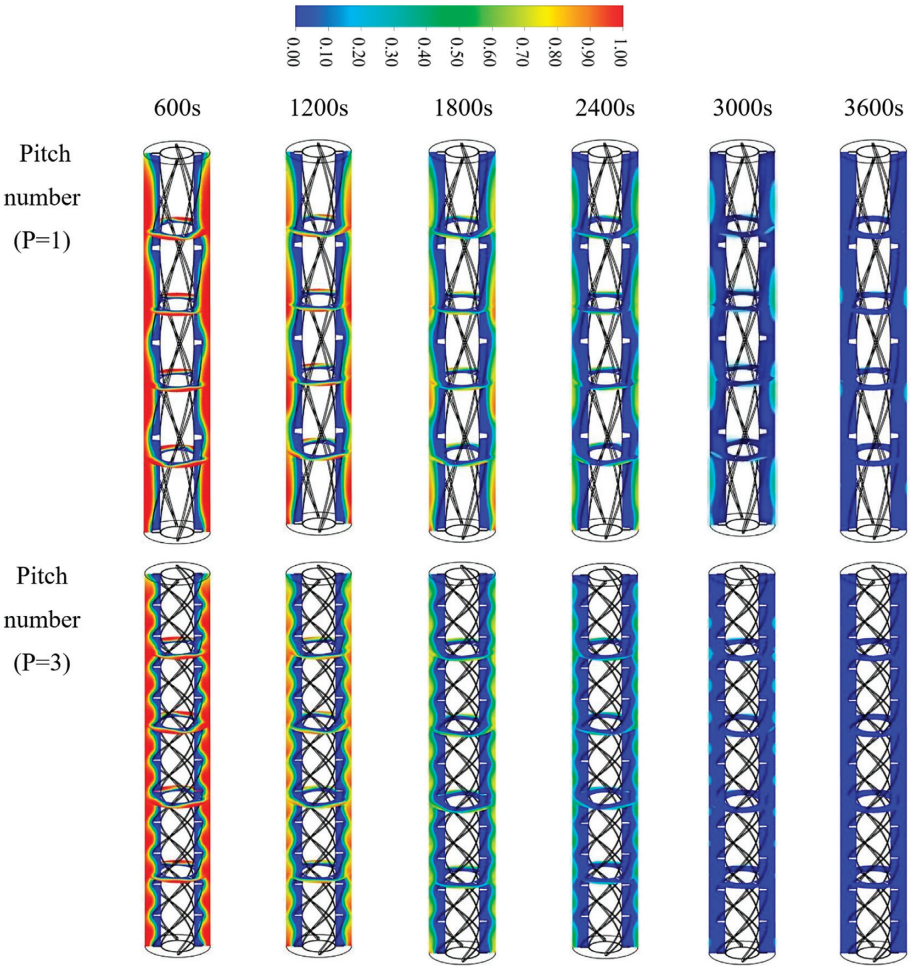

Figure 13: Liquid-fraction contours for fin pitch numbers (P = 1 and 3) over different solidification durations.

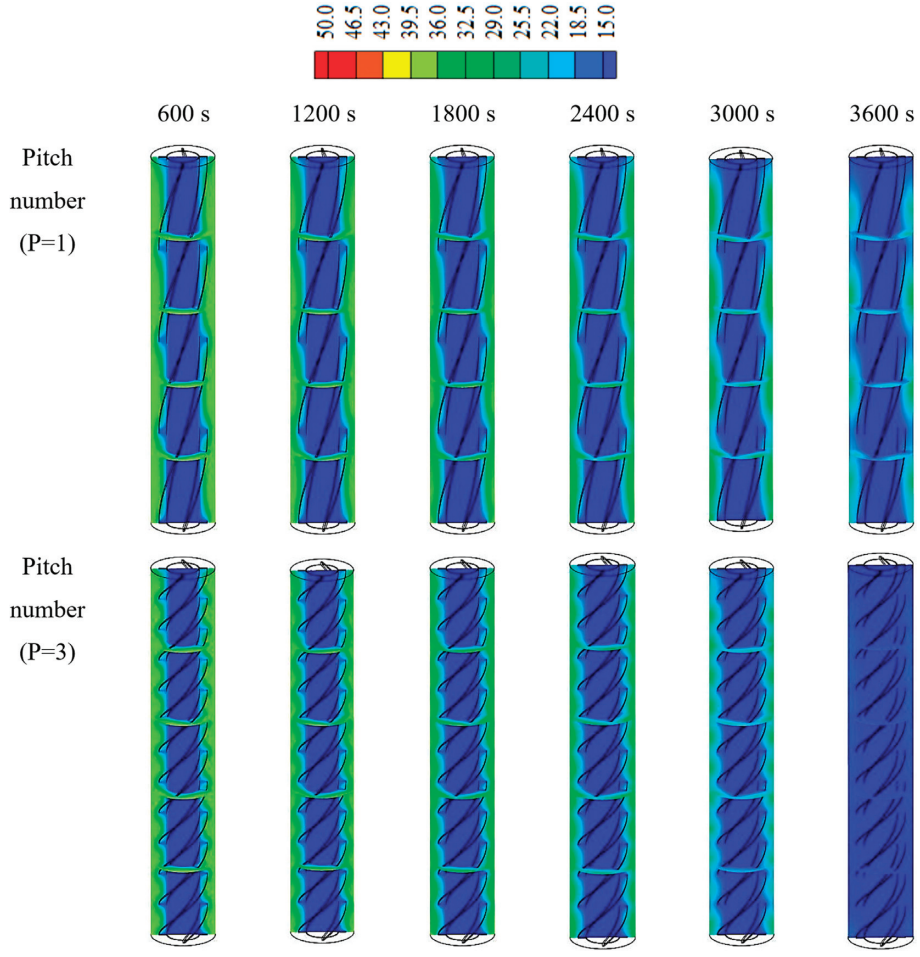

Figure 14: Temperature distribution contours for fin pitch numbers ($P = 1$ and 3) over different solidification durations.

distribution patterns. However, the isotherms began to move in less uniform patterns after 1800 s, indicating the appearance of a role for natural convection in the heat-transmission process. This distribution pattern was more pronounced in twisted fins with a smaller fin pitch. Although twisted fins with smaller pitches may improve natural convection, which serves as an additional source of heat removal from the liquid PCM, conduction remains the dominating heat-transport mechanism throughout the solidification process. This can be seen during the final melting duration (i.e., 3000–3600 s). Isotherms seem to be more uniform and consistent in color compared to the earlier solidifying durations, as a sign of the dominating role of conduction. Compared to the fin pitch of 1, twisted fins with a pitch of 3 appear to have more uniform isotherms with lower temperatures below 320 K (the blue zones) at most parts of the PCM domain during this duration of the process. This suggests that increasing the fin pitch results in closer fins that in turn aid faster heat-removal rates and consequently lower PCM temperatures during the solidification mode.

Figures 15 and 16 show the influence of fin pitches on the temporal liquid-fraction profile and the PCM temperature variation during solidification. As seen in Fig. 15, the liquid-fraction rate decreases as fin pitch increases. When fin pitch increases from 1 to 2 and from 1 to 3, the solidifying time decreases from 3600 s to about 3500 and 3200 s, respectively. Therefore, increasing the fin pitch from 1 to 2 decreases the solidifying time by ~3%, while

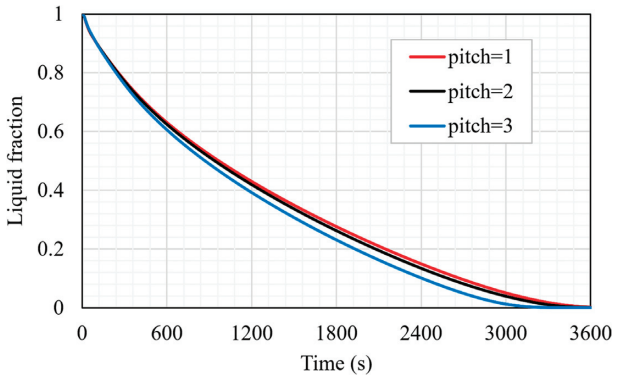

Figure 15: The temporal profiles of PCM liquid-fraction for three different cases of twisted-fin pitch number.

increasing the pitch from 1 to 3 reduces the solidifying time by ~11%. This implies that changing the fin pitch from 1 to 2 has a negligible impact on the PCM solidifying rate. Table 4 shows that the highest heat-retrieval rate for a pitch number of 3 is due to the higher heat-transfer area—corresponding to 11.60 W as compared to 11.37 and 11.25 W for pitch numbers of 2 and 1, respectively. This data indicates that the heat-removal rate can be improved by ~3.2 and ~1.0% compared to the base case of $P = 1$. In Fig. 15, it is observed that increasing the pitch number from 1 to 3 results

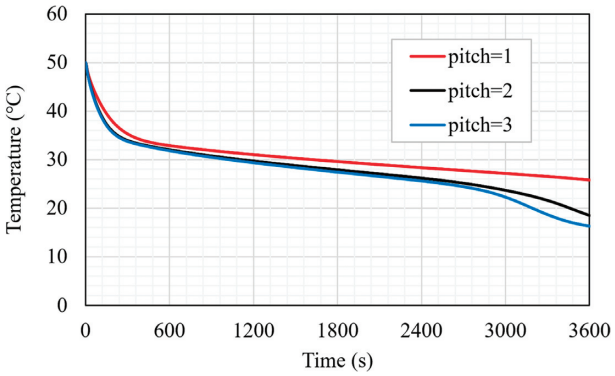

Figure 16: The temporal profiles of the average PCM temperature for three different cases of twisted-fin pitch number.

Table 4: The heat-retrieval rates during 3600 s of solidification for three different cases of twisted-fin pitch number.

Pitch number (*P*)	Heat-retrieval rate
1	11.25 W
2	11.37 W
3	11.60 W

in a significant temperature reduction but decreasing the pitch number from 2 to 3 results in a moderate reduction in the temperature. This is attributed to an increased heat exchange area between the HTF tube and the PCM, which is achieved by minimizing the gaps between twisted fins. Consequently, the highest possible fin pitch is favored for improving the solidification capacity of PCM.

5.4. Impact of fin thickness

Figure 17 shows the liquid-fraction contours for the effect of fin thickness in the case of twisted fins during six solidification durations of 600, 1200, 1800, 2400, 3000, and 3600 s. In the early duration of 600–1200 s, solidifying fronts (light green) appear to show larger waving along with forming distinct wave lines parallel to the fin walls. Increasing the fin thickness during this time appears to favor thicker solidifying layers (blue zones). The solidifying front proceeded to move significantly faster away from the twisted fin ligaments during 1800–2400 s. The difference in solidified PCM layers between the two cases of fin thickness is more pronounced than the previous duration. Increasing the fin thickness from 0.5 to 1.5 mm does not bring significant improvement to the solidification evolution during the whole process. The reason would be that employing thicker fins turns the spaces between them to be smaller. Thus, there is less volume available for accommodating the PCM between the fins, which aids the system to finish the solidifying process within shorter times. This behavior is more pronounced during the final duration of 3000–3600 s such that increasing fin thickness to 1.5 mm helps earlier termination of PCM solidification.

Figure 18 compares the isotherm distributions for the case of twisted fins with two different fin thicknesses. During the early duration of 600–1200 s, isotherms appear to be parallel and almost unified in color within the PCM domain due to conduction being the predominant mode of heat transfer. A change in fin thickness has no significant effect on the isotherm distribution patterns because conduction primarily governs heat removal from unsolidified PCM. In the second duration of 1800–2400 s, the isotherms begin to shift the major domain into more blue parts showing that natural convection began to play a role in heat transport. Fins with a smaller thickness show more prominent green zones in this distribution pattern. The reason for this is attributed to larger spaces for the buoyancy-driven flow of liquid PCM and better natural convection in twisted fins with smaller thicknesses. However, conduction remains the dominant heat-transport method during the whole process so that the changes in isotherm distribution patterns remain almost small or not significant between the two considered cases of fin thicknesses. These effects are more obvious in the final duration (i.e., 3000–3600 s). In comparison to previous solidifying durations, isotherms appear to be more uniform and stable in their color—indicating the dominance of conduction especially when the fin thickness is 1.5 mm, which appears to have a more uniform isotherm distribution.

Figures 19 and 20 depict the temporal liquid-fraction evolution and average PCM temperature of twisted fins with three different thicknesses during the solidification mode. The liquid-fraction evolution and PCM temperature are marginally affected by the fin thickness. As seen in Fig. 19, the solidifying time is around 3500 s for all fin thicknesses. This suggests that the PCM solidifying rate is not much affected by altering the fin thickness in the range of 0.5–1.5 mm. Table 5 shows that the fin thickness of 1.5 mm exhibits the highest heat-transmission area and heat-retrieval rate. In this case, PCM is faster cooled by twisted fins at the heat-retrieval rate of 11.47 W, while the other two cases with fin thickness of 0.5 and 1 mm can remove heat at lower rates of 11.37 and 11.25 W, respectively. Therefore, twisted fins with 1.5 and 1 mm thickness can improve heat removal by 2.1 and 1.2% compared to 0.5 mm, thickness, respectively.

6. Conclusions

In this paper, the discharging performance of RT35 PCM in a three-dimensional shell-and-tube LHTES system with the presence of twisted-fin arrays was numerically investigated. The system equipped with twisted tape was evaluative compared with the system with uniform longitudinal fins and a system without fins. The results showed that proceeding with time, the solidifying layer expanded quickly to the bottom part of the domain in case of twisted-fin configuration as compared to no fins and straight fin cases due to more effective conduction in this region. As such, the discharging time of the twisted fin was 36 and 13% lower than that for the systems with the no-fin case and straight fins. Moreover, the heat-removal rate for the system with twisted fins was reduced by 12 and 35.5% in comparison with the system equipped with straight fins and no-fins. Upon the successful outcome of the proposed concept, a parametric analysis was performed to estimate the effect of fin height, fin pitch number, and fin thickness – in the case of twisted-fin arrangement – on the liquid fraction, isotherm distribution contours, solidification time, and heat-transfer rate. The increase in the fin height from 2.5 to 7.5 mm was associated with a better heat diffusion in both vertical and angular directions due to a larger surface area of twisted fins—contributing to the enhancement in the conduction heat transfer in the PCM while minimizing the natural convection by the generated flow-resistant forces. This was evidenced by comparing the contours of temperature distribution for these cases. As a case in point, the heat-retrieval rate was increased from 10.0 to 11.4 W and the discharging time was de-

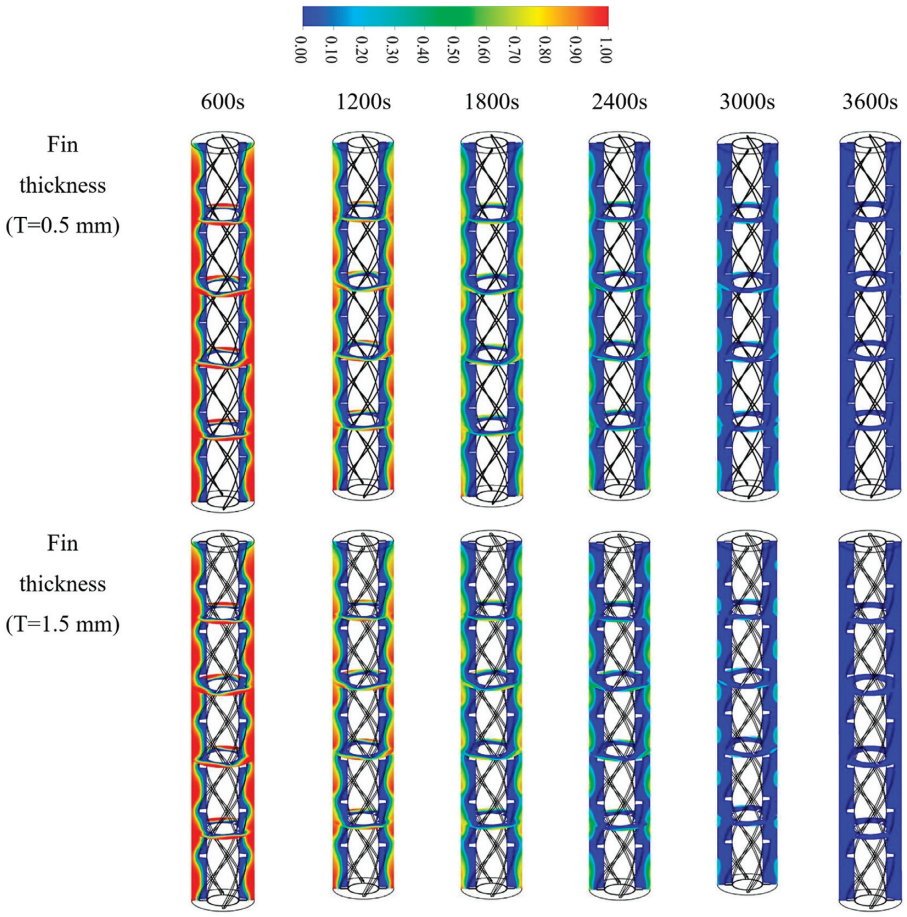

Figure 17: Liquid-fraction contours for fin thicknesses ($T = 0.5$ and 1.5 mm) over different solidification durations.

creased from above 3600 to 2880 s by increasing the fin height from 2.5 to 7.5 mm. The heat-discharge rate and solidification time were improved by the pitch number which is less effective compared with that of the fin height. The increase in the pitch number from 1 to 3 intensified the heat-removal rate by ~3% and reduced the solidification time by ~9%. In the case of fin thickness, the results demonstrated a marginal improvement in the heat-retrieval rate and discharging time by increasing the fin thickness. The charging/discharging performance of twisted-fin configuration can be further enhanced by changing the arrangement of twisted fins (staggered versus non-staggered alignment), considering the non-uniform fin length, and adding porosity to the fin surface—recommendations for future topics in this realm. Furthermore, the effective parameters can be optimized as a further investigation using computational intelligence algorithms such as monarch butterfly optimization (Wang *et al.*, 2019), earthworm optimization algorithm (Ghosh & Roy, 2019), elephant herding optimization (Wang *et al.*, 2015), etc., to further enhance the performance of thermal storage unit.

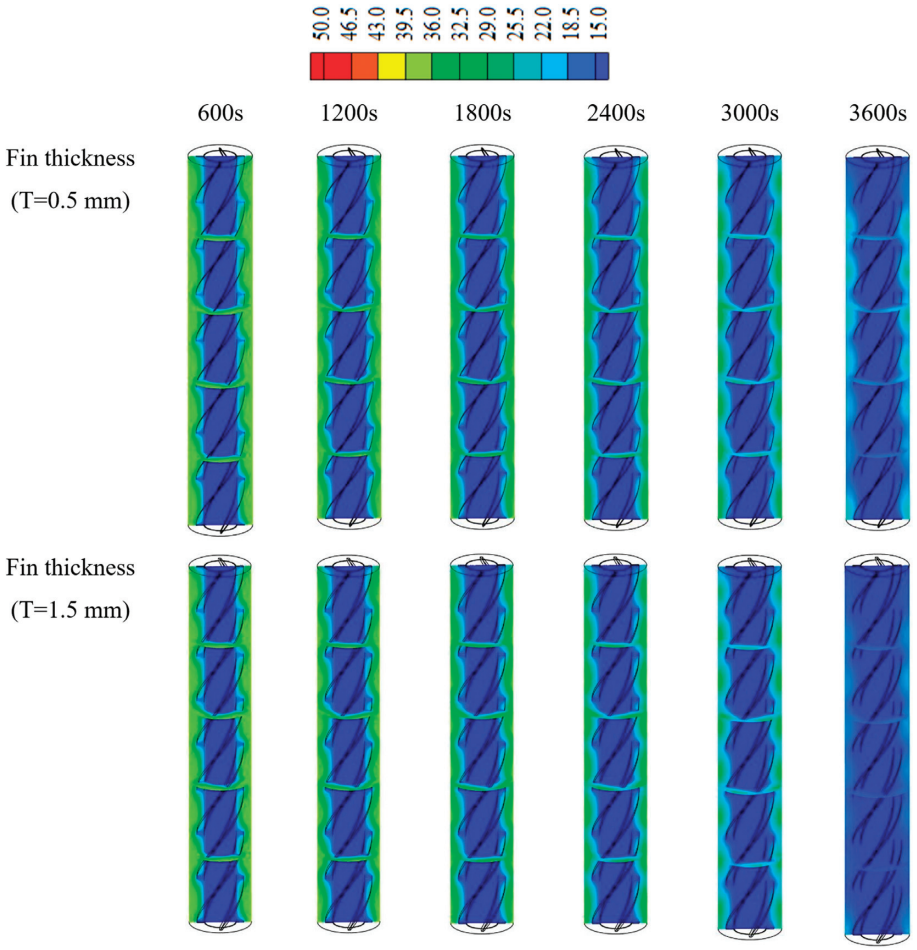

Figure 18: Temperature distribution contours for fin thicknesses (T = 0.5 and 1.5 mm) over different solidification durations.

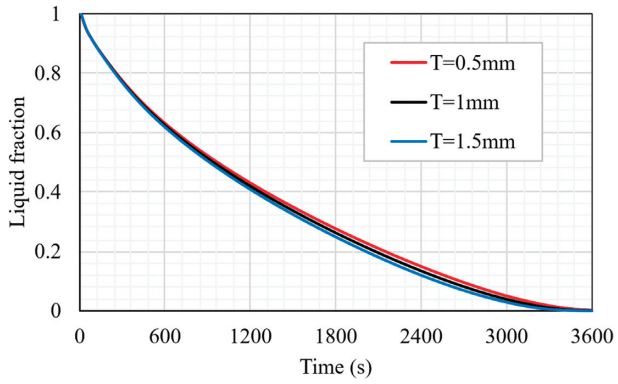

Figure 19: The temporal profiles of PCM liquid-fraction for three different cases of twisted-fin thickness.

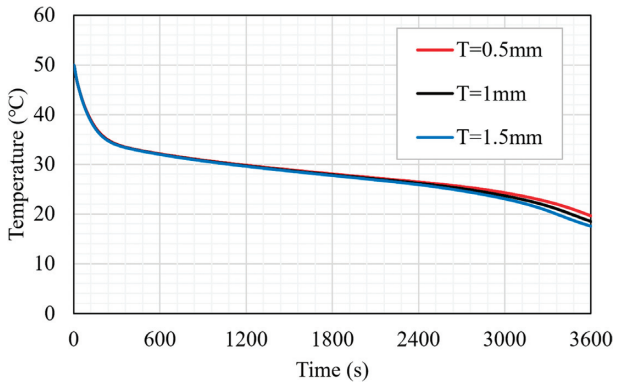

Figure 20: The temporal profiles of the average PCM temperature for three different cases of twisted-fin thickness.

Table 5: The heat-retrieval rates during 3600 s of solidification for three different cases of twisted-fin thickness.

Fin thickness (T)	Heat-retrieval rate
0.5 mm	11.25 W
1.0 mm	11.37 W
1.5 mm	11.47 W

Acknowledgments

The authors gratefully acknowledge the National Science Foundation of China (Grant No. 51904233), the National Science Foundation of China (Grant No.52074218), and the Innovation Capability Support Program of Shannxi Province (Grant No. 2020TD- 021)

Conflict of interest statement

None declared.

References

Abdulateef, A. M., Mat, S., Sopian, K., Abdulateef, J., & Gitan, A. A. (2017). Experimental and computational study of melting phase-change material in a triplex tube heat exchanger with longitudinal/triangular fins. *Solar Energy*, **155**, 142–153. https://doi.org/10.1016/j.solener.2017.06.024.

Abdulateef, A. M., Abdulateef, J., Mat, S., Sopian, K., Elhub, B., & Mussa, M. A. (2018). Experimental and numerical study of solidifying phase-change material in a triplex-tube heat exchanger with longitudinal/triangular fins. *International Communications in Heat and Mass Transfer*, **90**, 73–84. https://doi.org/10.1016/j.icheatmasstransfer.2017.10.003.

Agyenim, F., Eames, P., & Smyth, M. (2009). A comparison of heat transfer enhancement in a medium temperature thermal energy storage heat exchanger using fins. *Solar Energy*, **83**, 1509–1520. https://doi.org/10.1016/j.solener.2009.04.007.

Agyenim, F., Hewitt, N., Eames, P., & Smyth, M. (2010). A review of materials, heat transfer and phase change problem formulation for latent heat thermal energy storage systems (LHTESS). *Renewable and Sustainable Energy Reviews*, **14**, 615–628. https://doi.org/10.1016/j.rser.2009.10.015.

Al-Abidi, A. A., Mat, S., Sopian, K., Sulaiman, M., & Mohammad, A. T. (2013a). Internal and external fin heat transfer enhancement technique for latent heat thermal energy storage in triplex tube heat exchangers. *Applied Thermal Engineering*, **53**, 147–156. https://doi.org/10.1016/j.applthermaleng.2013.01.011.

Al-Abidi, A. A., Mat, S., Sopian, K., Sulaiman, M., & Mohammad, A. T. (2013b). Numerical study of PCM solidification in a triplex tube heat exchanger with internal and external fins. *International Journal of Heat and Mass Transfer*, **61**, 684–695. https://doi.org/10.1016/j.ijheatmasstransfer.2013.02.030.

Al-Abidi, A. A., Mat, S., Sopian, K., Sulaiman, M. Y., & Mohammad, A. T. (2014). Experimental study of melting and solidification of PCM in a triplex tube heat exchanger with fins. *Energy and Buildings*, **68**, 33–41. https://doi.org/10.1016/j.enbuild.2013.09.007.

Arasteh, H., Rahbari, A., Mashayekhi, R., Keshmiri, A., Mahani, R. B., & Talebizadehsardari, P. (2021). Effect of pitch distance of rotational twisted tape on the heat transfer and fluid flow characteristics. *International Journal of Thermal Sciences*, **170**, 106966. https://doi.org/10.1016/j.ijthermalsci.2021.106966.

Chavan, S., Rudrapati, R., & Manickam, S. (2022). A comprehensive review on current advances of thermal energy storage and its applications. *Alexandria Engineering Journal*, **61**, 5455–5463. https://doi.org/10.1016/j.aej.2021.11.003.

Elmaazouzi, Z., Laasri, I. A., Gounni, A., & El Alami, M. (2021). Enhanced thermal performance of finned latent heat thermal energy storage system: Fin parameters optimization. *Journal of Energy Storage*, **43**, 103116. https://doi.org/10.1016/j.est.2021.103116.

Erek, A., İlken, Z., & Acar, M. A. (2005). Experimental and numerical investigation of thermal energy storage with a finned tube. *International Journal of Energy Research*, **29**, 283–301. https://doi.org/10.1002/er.1057.

Fadl, M., & Eames, P. C. (2019). Numerical investigation of the influence of mushy zone parameter amush on heat transfer characteristics in vertically and horizontally oriented thermal energy storage systems. *Applied Thermal Engineering*, **151**, 90–99. https://doi.org/10.1016/j.applthermaleng.2019.01.102.

Farid, M. M., Khudhair, A. M., Razack, S. A. K., & Al-Hallaj, S. (2004). A review on phase change energy storage: Materials and applications. *Energy Conversion and Management*, **45**, 1597–1615. https://doi.org/10.1016/j.enconman.2003.09.015.

Gao, D., Wang, G. G., & Pedrycz, W. (2020). Solving fuzzy job-shop scheduling problem using DE algorithm improved by a selection mechanism. *IEEE Transactions on Fuzzy Systems*, **28**, 3265–3275. https://doi.org/10.1109/TFUZZ.2020.3003506.

Ghalambaz, M., Groşan, T., & Pop, I. (2019). Mixed convection boundary layer flow and heat transfer over a vertical plate embedded in a porous medium filled with a suspension of nano-encapsulated phase change materials. *Journal of Molecular Liquids*, **293**, 111432. https://doi.org/10.1016/j.molliq.2019.111432.

Ghalambaz, M., Zadeh, S. M. H., Mehryan, S., Pop, I., & Wen, D. (2020). Analysis of melting behavior of PCMs in a cavity subject to a non-uniform magnetic field using a moving grid technique. *Applied Mathematical Modelling*, **77**, 1936–1953. https://doi.org/10.1016/j.apm.2019.09.015.

Ghalambaz, M., Mahdi, J. M., Shafaghat, A., Eisapour, A. H., Younis, O., Talebizadeh Sardari, P., & Yaïci, W. (2021a). Effect of twisted fin array in a triple-tube latent heat storage system during the charging mode. *Sustainability*, **13**, 2685. https://doi.org/10.3390/su13052685.

Ghalambaz, M., Mohammed, H. I., Mahdi, J. M., Eisapour, A. H., Younis, O., Ghosh, A., Talebizadehsardari, P., & Yaïci, W. (2021b). Intensifying the charging response of a phase-change material with twisted fin arrays in a shell-and-tube storage system. *Energies*, **14**, 1619. https://doi.org/10.3390/en14061619.

Ghalambaz, M., & Zhang, J. (2020). Conjugate solid-liquid phase change heat transfer in heatsink filled with phase change material-metal foam. *International Journal of Heat and Mass Transfer*, **146**, 118832. https://doi.org/10.1016/j.ijheatmasstransfer.2019.118832.

Ghosh, I., & Roy, P. K.. (2019). *Application of earthworm optimization algorithm for solution of optimal power flow*. In Proceedings of 2019 International Conference on Opto-Electronics and Applied Optics (Optronix)(pp. 1–6). https://doi.org/10.1109/OPTRONIX.2019.8862335.

Hassan, A. K., Abdulateef, J., Mahdi, M. S., & Hasan, A. F. (2020). Experimental evaluation of thermal performance of two different finned latent heat storage systems. *Case Studies in Thermal Engineering*, **21**, 100675. https://doi.org/10.1016/j.csite.2020.100675.

He, J., Liu, X., Zhao, Y., Du, H., Zhang, T., & Shi, J. (2022). Dielectric stability and energy-storage performance of BNT-based relaxor ferroelectrics through Nb5+ and its excess modification. *ACS Applied Electronic Materials*, **4**, 735–743. https://doi.org/10.1021/acsaelm.1c01129.

Hosseinzadeh, K., Alizadeh, M., & Ganji, D. (2019). Solidification process of hybrid nano-enhanced phase change material in a LHTESS with tree-like branching fin in the presence of thermal radiation. *Journal of Molecular Liquids*, **275**, 909–925. https://doi.org/10.1016/j.molliq.2018.11.109.

Hosseinzadeh, K., Montazer, E., Shafii, M. B., & Ganji, A. (2021). Solidification enhancement in triplex thermal energy storage system via triplets fins configuration and hybrid nanoparticles. *Journal of Energy Storage*, **34**, 102177. https://doi.org/10.1016/j.est.2020.102177.

Huang, Y., & Liu, X. (2021). Charging and discharging enhancement of a vertical latent heat storage unit by fractal tree-shaped fins. *Renewable Energy*, **174**, 199–217. https://doi.org/10.1016/j.renene.2021.04.066.

Huang, X., & Yao, S. (2021). Solidification performance of new trapezoidal longitudinal fins in latent heat thermal energy storage. *Case Studies in Thermal Engineering*, **26**, 101110. https://doi.org/10.1016/j.csite.2021.101110.

IEA. (2021). *Key World Energy Statistics 2021*. Technical report. IEA, Paris. https://www.iea.org/reports/key-world-energy-statistics-2021.

Ibrahim, N. I., Al-Sulaiman, F. A., Rahman, S., Yilbas, B. S., & Sahin, A. Z. (2017). Heat transfer enhancement of phase change materials for thermal energy storage applications: A critical review. *Renewable and Sustainable Energy Reviews*, **74**, 26–50. https://doi.org/10.1016/j.rser.2017.01.169.

Jmal, I., & Baccar, M. (2015). Numerical study of PCM solidification in a finned tube thermal storage including natural convection. *Applied Thermal Engineering*, **84**, 320–330. https://doi.org/10.1016/j.applthermaleng.2015.03.065.

Jmal, I., & Baccar, M. (2018). Numerical investigation of PCM solidification in a finned rectangular heat exchanger including natural convection. *International Journal of Heat and Mass Transfer*, **127**, 714–727. https://doi.org/10.1016/j.ijheatmasstransfer.2018.08.058.

Li, M., & Wang, G. G. (2022). A review of green shop scheduling problem. *Information Sciences*, **589**, 478–496. https://doi.org/10.1016/j.ins.2021.12.122.

Liu, Z., Liu, Z., Guo, J., Wang, F., Yang, X., & Yan, J. (2022). Innovative ladder-shaped fin design on a latent heat storage device for waste heat recovery. *Applied Energy*, **321**, 119300. https://doi.org/10.1016/j.apenergy.2022.119300.

Lu, B., Zhang, Y., Sun, D., Yuan, Z., & Yang, S. (2021). Experimental investigation on thermal behavior of paraffin in a vertical shell and spiral fin tube latent heat thermal energy storage unit. *Applied Thermal Engineering*, **187**, 116575. https://doi.org/10.1016/j.applthermaleng.2021.116575.

Luo, Y., Xie, Y., Geng, W., Chu, J., Wu, H., Xie, D., Sheng, X., & Mei, Y. (2022). Boosting fire safety and mechanical performance of thermoplastic polyurethane by the face-to-face two-dimensional phosphorene/MXene architecture. *Journal of Materials Science & Technology*, **129**, 27–39. https://doi.org/10.1016/j.jmst.2022.05.003.

Mahdi, J. M., Lohrasbi, S., Ganji, D. D., & Nsofor, E. C. (2018). Accelerated melting of PCM in energy storage systems via novel configuration of fins in the triplex-tube heat exchanger. *International Journal of Heat and Mass Transfer*, **124**, 663–676. https://doi.org/10.1016/j.ijheatmasstransfer.2018.03.095.

Mahdi, J. M., Lohrasbi, S., & Nsofor, E. C. (2019). Hybrid heat transfer enhancement for latent-heat thermal energy storage systems: A review. *International Journal of Heat and Mass Transfer*, **137**, 630–649. https://doi.org/10.1016/j.ijheatmasstransfer.2019.03.111.

Mahdi, J. M., & Nsofor, E. C. (2016). Solidification of a PCM with nanoparticles in triplex-tube thermal energy storage system. *Applied Thermal Engineering*, **108**, 596–604. https://doi.org/10.1016/j.applthermaleng.2016.07.130.

Mahdi, J. M., & Nsofor, E. C. (2017a). Melting enhancement in triplex-tube latent thermal energy storage system using nanoparticles-fins combination. *International Journal of Heat and Mass Transfer*, **109**, 417–427. https://doi.org/10.1016/j.ijheatmasstransfer.2017.02.016.

Mahdi, J. M., & Nsofor, E. C. (2017b). Solidification enhancement in a triplex-tube latent heat energy storage system using nanoparticles-metal foam combination. *Energy*, **126**, 501–512. https://doi.org/10.1016/j.energy.2017.03.060.

Mahdi, J. M., & Nsofor, E. C. (2018). Solidification enhancement of PCM in a triplex-tube thermal energy storage system with nanoparticles and fins. *Applied Energy*, **211**, 975–986. https://doi.org/10.1016/j.apenergy.2017.11.082.

Mahmood, A. S. (2019). Experimental study on double-pass solar air heater with and without using phase change material. *Journal of Engineering*, **25**, 1–17. https://doi.org/10.31026/j.eng.2019.02.01.

Mashayekhi, R., Arasteh, H., Talebizadehsardari, P., Kumar, A., Hangi, M., & Rahbari, A. (2022a). Heat transfer enhancement of nanofluid flow in a tube equipped with rotating twisted tape inserts: A two-phase approach. *Heat Transfer Engineering*, **43**, 608–622. https://doi.org/10.1080/01457632.2021.1896835.

Mashayekhi, R., Eisapour, A. H., Eisapour, M., Talebizadehsardari, P., & Rahbari, A. (2022b). Hydrothermal performance of twisted elliptical tube equipped with twisted tape insert. *International Journal of Thermal Sciences*, **172**, 107233. https://doi.org/10.1016/j.ijthermalsci.2021.107233.

Mehta, D. S., Vaghela, B., Rathod, M. K., & Banerjee, J. (2021). Heat transfer enhancement using spiral fins in different orientations of latent heat storage unit. *International Journal of Thermal Sciences*, **169**, 107060. https://doi.org/10.1016/j.ijthermalsci.2021.107060.

Nóbrega, C. R., Ismail, K. A., & Lino, F. A. (2019). Correlations for predicting the performance of axial finned tubes submersed in PCM. *Journal of Energy Storage*, **26**, 100973. https://doi.org/10.1016/j.est.2019.100973.

Nóbrega, C. R., Ismail, K. A., & Lino, F. A. (2020). Solidification around axial finned tube submersed in PCM: Modeling and experiments. *Journal of Energy Storage*, **29**, 101438. https://doi.org/10.1016/j.est.2020.101438.

Patel, J. R., & Rathod, M. K. (2019). Thermal performance enhancement of melting and solidification process of phase-change material in triplex tube heat exchanger using longitudinal fins. *Heat Transfer—Asian Research*, **48**, 483–501. https://doi.org/10.1002/htj.21372.

Pu, L., Zhang, S., Xu, L., & Li, Y. (2020). Thermal performance optimization and evaluation of a radial finned shell-and-tube latent heat thermal energy storage unit. *Applied Thermal Engineering*, **166**, 114753. https://doi.org/10.1016/j.applthermaleng.2019.114753.

Reddy, K., Mudgal, V., & Mallick, T. (2018). Review of latent heat thermal energy storage for improved material stability and effective load management. *Journal of Energy Storage*, **15**, 205–227. https://doi.org/10.1016/j.est.2017.11.005.

Rubitherm. (2020). Product information, data sheet of RT35. https://www.rubitherm.eu.

Talebizadeh Sardari, P., Walker, G. S., Gillott, M., Grant, D., & Giddings, D. (2020). Numerical modelling of phase change material melting process embedded in porous media: Effect of heat storage size. *Proceedings of the Institution of Mechanical Engineers, Part A: Journal of Power and Energy*, **234**, 365–383. https://doi.org/10.1177%2F0957650919862974.

Shahsavar, A., Talebizadeh, P., & Tabaei, H. (2013). Optimization with genetic algorithm of a PV/T air collector with natural air flow and a case study. *Journal of Renewable and Sustainable Energy*, **5**, 023118. https://doi.org/10.1063/1.4798312.

Shahsavar, A., Shaham, A., & Talebizadehsardari, P. (2019a). Wavy channels triple-tube LHS unit with sinusoidal variable wavelength in charging/discharging mechanism. *International Communications in Heat and Mass Transfer*, **107**, 93–105. https://doi.org/10.1016/j.icheatmasstransfer.2019.05.012

Shahsavar, A., Al-Rashed, A. A., Entezari, S., & Sardari, P. T. (2019b). Melting and solidification characteristics of a double-pipe latent

heat storage system with sinusoidal wavy channels embedded in a porous medium. *Energy*, **171**, 751–769. https://doi.org/10.1016/j.energy.2019.01.045.

Shahsavar, A., Majidzadeh, A. H., Mahani, R. B., & Talebizadehsardari, P. (2021). Entropy and thermal performance analysis of PCM melting and solidification mechanisms in a wavy channel triplex-tube heat exchanger. *Renewable Energy*, **165**, 52–72. https://doi.org/10.1016/j.renene.2020.11.074.

Shahsavar, A., Alwaeli, A. H. A., Azimi, N., Rostami, S., Sopian, K., Arıcı, M., Estellé, P., Nižetić, S., Kasaeian, A., Ali, H. M., Mak, Z., & Afrand, M. (2022). Exergy studies in water-based and nanofluid-based photovoltaic/thermal collectors: Status and prospects. *Renewable and Sustainable Energy Reviews*, **168**, 112740. https://doi.org/10.1016/j.rser.2022.112740.

Shahsavari, A., & Akbari, M. (2018). Potential of solar energy in developing countries for reducing energy-related emissions. *Renewable and Sustainable Energy Reviews*, **90**, 275–291. https://doi.org/10.1016/j.rser.2018.03.065.

Sharma, A., Tyagi, V., Chen, C., & Buddhi, D. (2009). Review on thermal energy storage with phase change materials and applications. *Renewable and Sustainable Energy Reviews*, **13**, 318–345. https://doi.org/10.1016/j.rser.2007.10.005.

Shi, J., Zhao, Y., He, J., Li, T., Zhu, F., Tian, W., & Liu, X. (2022). Deferred polarization saturation boosting superior energy-storage efficiency and density simultaneously under moderate electric field in relaxor ferroelectrics. *ACS Applied Energy Materials*, **5**, 3436–3446. https://doi.org/10.1021/acsaem.1c04017.

Tiari, S., Hockins, A., & Mahdavi, M. (2021). Numerical study of a latent heat thermal energy storage system enhanced by varying fin configurations. *Case Studies in Thermal Engineering*, **25**, 100999. https://doi.org/10.1016/j.csite.2021.100999.

Wang, G., & Tan, Y. (2019). Improving metaheuristic algorithms with information feedback models. *IEEE Transactions on Cybernetics*, **49**, 542–555. https://doi.org/10.1109/TCYB.2017.2780274.

Wang, G. G., Deb, S., & Coelho, L. D. S. (2015). *Elephant herding optimization*. In Proceedings of 2015 3rd International Symposium on Computational and Business Intelligence (ISCBI)(pp. 1–5). https://doi.org/10.1109/ISCBI.2015.8.

Wang, M., Jiang, C., Zhang, S., Song, X., Tang, Y., & Cheng, H. M. (2018). Reversible calcium alloying enables a practical room-temperature rechargeable calcium-ion battery with a high discharge voltage. *Nature Chemistry*, **10**, 667–672. https://doi.org/10.1038/s41557-018-0045-4.

Wang, G. G., Deb, S., & Cui, Z. (2019). Monarch butterfly optimization. *Neural Computing and Applications*, **31**, 1995–2014.

Wang, G. G., Gao, D., & Pedrycz, W. (2022). Solving multi-objective fuzzy job-shop scheduling problem by a hybrid adaptive differential evolution algorithm. *IEEE Transactions on Industrial Informatics*, **18**, 8519–8528. https://doi.org/10.1109/TII.2022.3165636.

Wang, Z., Wang, Q., Jia, C., & Bai, J. (2022). Thermal evolution of chemical structure and mechanism of oil sands bitumen. *Energy*, **244**, 123190. https://doi.org/10.1016/j.energy.2022.123190.

Wu, H., Hu, X., Li, X., Sheng, M., Sheng, X., Lu, X., & Qu, J. (2022). Large-scale fabrication of flexible EPDM/MXene/PW phase change composites with excellent light-to-thermal conversion efficiency via water-assisted melt blending. *Composites Part A: Applied Science and Manufacturing*, **152**, 106713. https://doi.org/10.1016/j.compositesa.2021.106713.

Xu, Y., Ren, Q., Zheng, Z. J., & He, Y. L. (2017). Evaluation and optimization of melting performance for a latent heat thermal energy storage unit partially filled with porous media. *Applied Energy*, **193**, 84–95. https://doi.org/10.1016/j.apenergy.2017.02.019.

Yan, W. T., Li, C., & Ye, W. B. (2019). Numerical investigation of hydrodynamic and heat transfer performances of nanofluids in a fractal microchannel heat sink. *Heat Transfer—Asian Research*, **48**, 2329–2349. https://doi.org/10.1002/htj.21494.

Yan, W., Feng, G., Luo, X., Hu, Y. Q., Guo, J., Yu, Z., Zhao, Z., & Ding, S. (2022). Singlet oxygen-promoted one-pot synthesis of highly ordered mesoporous silica materials via the radical route. *Green Chemistry*, **24**, 4778–4782. https://doi.org/10.1039/D2GC00869F.

Yang, X., Lu, Z., Bai, Q., Zhang, Q., Jin, L., & Yan, J. (2017). Thermal performance of a shell-and-tube latent heat thermal energy storage unit: role of annular fins. *Applied Energy*, **202**, 558–570. https://doi.org/10.1016/j.apenergy.2017.05.007.

Yang, X., Guo, J., Yang, B., Cheng, H., Wei, P., & He, Y. L. (2020). Design of non-uniformly distributed annular fins for a shell-and-tube thermal energy storage unit. *Applied Energy*, **279**, 115772. https://doi.org/10.1016/j.apenergy.2020.115772.

Ye, W. B. (2016). Thermal simulation and evaluation for non-uniformity detection of electrode. *Applied Thermal Engineering*, **96**, 583–592. https://doi.org/10.1016/j.applthermaleng.2015.12.007.

Ye, W. B. (2017). Finite volume analysis the thermal behavior of electrode non-uniformity. *Heat and Mass Transfer*, **53**, 1123–1132. https://doi.org/10.1007/s00231-016-1879-1.

Ye, W. B., Li, C., Huang, S. M., & Hong, Y. (2019). Validation of thermal modeling of unsteady heat source generated in a rectangular lithium-ion power battery. *Heat Transfer Research*, **50**, 233–241. https://doi.org/10.1615/HeatTransRes.2018026809.

Youssef, W., Ge, Y., & Tassou, S. (2018). CFD modelling development and experimental validation of a phase change material (PCM) heat exchanger with spiral-wired tubes. *Energy Conversion and Management*, **157**, 498–510. https://doi.org/10.1016/j.enconman.2017.12.036.

Zhang, X., Tang, Y., Zhang, F., & Lee, C. S. (2016). A novel aluminum–graphite dual-ion battery. *Advanced Energy Materials*, **6**, 1502588. https://doi.org/10.1002/aenm.201502588.